International Journal of Bioprinting

RESEARCH ARTICLE

Valorization of agar production residue as a filler in soy protein hydrogels for 3D printing

Jone Uranga[1], Teresa Carranza[1], Miriam Peñalba[1], Koro de la Caba[1,2]*, Pedro Guerrero[1,2,3]*

[1]BIOMAT Research Group, University of the Basque Country (UPV/EHU), Escuela de Ingeniería de Gipuzkoa, Plaza de Europa 1, 20018 Donostia-San Sebastián, Spain

[2]BCMaterials, Basque Center for Materials, Applications and Nanostructures, UPV/EHU Science Park, 48940, Leioa, Spain

[3]Proteinmat Materials SL, Avenida de Tolosa 72, 20018 Donostia-San Sebastián, Spain

(This article belongs to the *Special Issue: Novel hydrogels/bioinks formulations prepared from naturally derived components for 3D Bioprinting*)

Abstract

Cellulose-containing residue from agar production was incorporated as a filler into soy protein-based hydrogels and revalorized without further purification. Rheological assessment of these hydrogels was carried out in order to confirm their shear-thinning behavior and their suitability for 3D printing. It was observed that all hydrogels behaved as weak gels, which are suitable for 3D printing and have good printability and shape fidelity. The addition of cellulose did not cause chemical crosslinking but physical interactions, which led to morphological changes, thereby promoting hardness and shape recovery of the 3D-printed products. The hydrogel with the highest residue content (8 wt %) showed the highest value (78%) in shape recovery. Furthermore, the physicochemical characterization of these 3D-printed products revealed that although they have high swelling capacity, they preserve their integrity in wet conditions. These results suggested the potential of the 3D-printed products developed using residues without further purification to promote circular economy, increasing the efficiency in resources utilization.

Keywords: Hydrogels; Proteins; Cellulose; Rheology; 3D printing

***Corresponding authors:**
Pedro Guerrero
(pedromanuel.guerrero@ehu.es)

Koro de la Caba
(koro.delacaba@ehu.es)

Citation: Uranga J, Carranza T, Peñalba M, *et al*., 2023, Valorization of agar production residue as a filler in soy protein hydrogels for 3D printing. *Int J Bioprint,* 9(4): 731. https://doi.org/10.18063/ijb.731

Received: February 03, 2023
Accepted: March 05, 2023
Published Online: April 10, 2023

1. Introduction

Population growth, diversification of individual consumption, urban concentration, increasing number of industries, and lack of strategies for treating waste all contribute to many problems associated with the environment and human health. In line with circular economy and zero-waste discharge policies, one of the emerging tendencies in recent years is to prepare novel and environmentally-friendly materials such as residues from industry[1-3]. In this context, the exploitation of red algae, especially *Gelidium sesquipedale*, which is widely available around the world, for the production of agar products is important for several industries, ranging from cosmetics to the food industry[4]. The industrial processing of red algae generates a large quantity of solid fibrous wastes, which constitute a source of serious environmental problems. The agar extraction process produces a substantial amount of residue (15%–40% of the initial

dry biomass), which is currently underutilized, but they are mostly discarded or used as soil fertilizer[5,6]. Indeed, this algal waste exists in large quantities but its valorization to produce highly value-added materials has not yet been performed. After agar–agar extraction, the remaining algal waste consists of 87.4% organic matter, mainly cellulose and proteins. Marine biomass, especially algae derivatives, contains a higher yield of carbohydrates[7]; therefore, employing these residues in the manufacturing of bio-based materials could be a strategy for adding value to this waste stream.

Many reported studies are focused on cellulose purification, and the pretreatment, separation, and functionalization of cellulose can be complex and can generate harmful byproducts[8]. Chlorine and ammonia leakage, odor, ground water pollution, toxicity, and generation of carcinogens are some of the possible flaws of these cellulose purification methods. Acid hydrolysis is considered the safest extraction method but this procedure could still cause harmful effects on the environment. Therefore, applying simplified extraction procedures, or even no extraction, may be beneficial from an economical and environmental perspective. One method to produce materials with cellulose without any modification process is the preparation of hydrogels. Hydrogels derived from natural polymers, especially polysaccharides, are very attractive materials since they have applications in many fields (agriculture, tissue engineering, drug delivery, biosensors). Additionally, another advantage is that they are prepared from environmentally friendly, renewable and inexpensive raw materials. This was the approach followed in this work, where the residue obtained from the agar production, comprising mainly cellulose and proteins, was incorporated as a filler into protein-based formulations. Employing this residue is intended to achieve two objectives: (i) to conceive, a more effective waste disposal strategy, and (ii) to generate value-added products with lower cost.

Cellulose and its derivatives are often blended with other biopolymers to enhance properties[9,10]. Biopolymers in this regard include proteins, such as soy protein, a vegetal protein that contains abundant polar groups such as carboxyl, amine, and hydroxyl groups, which facilitate conjugation with other molecules[11]. These mixtures can be processed by various methods, including 3D printing[12]. One of the major hurdles that limit the widespread application of 3D printing is the lack of diverse biomaterial inks with appropriate printability[13]. Therefore, the objective of this work is to verify the printability of natural inks developed from agar residue in line with circular economy principles. Considering that printability is dependent on the material rheological properties, other biopolymers, such as gelatin, can be employed to achieve the required viscosity for the 3D printing process[14]. In this work, soy protein-based products, with gelatin and agar production residue as additives, were prepared by 3D printing. First, rheological and printability assessments of the hydrogels were conducted to study the effect of the residue content on 3D printing. Furthermore, the characterization of the 3D-printed products was performed to relate their structure to their physicochemical, thermal, and mechanical properties.

2. Materials and methods

2.1. Materials

Soy protein isolate (SPI) PROFAM 974 (ADM Protein Specialties Division, the Netherlands), cellulose (C)-containing residue from agar production (Roko agar, Spain), porcine gelatin with 280 bloom (Sancho de Borja, Spain), and glycerol (Panreac, Spain) were used for the hydrogel formulations. All chemicals were used as-received without further purification. Phosphate-buffered saline (PBS; Sigma-Aldrich, USA) was used for the swelling and degradation study.

2.2. Preparation of hydrogels

Hydrogels were prepared by mixing SPI 50% w/v in 50 mL distilled water, together with 5 wt % porcine gelatin, 0, 2, 4, 6 or 8 wt % milled cellulose-containing residue, and 20 wt % glycerol; all of them are based on SPI mass. Mixtures were kept at 80°C under constant stirring for 20 min. Afterward, the pH was adjusted to 7 using NaOH (1 M), and the mixing procedure (80°C, 20 min) was repeated. Then, the sample was stirred at 8000 rpm for 250 s with an IKA S 25N-18G-ST ULTRA-TURRAX homogenizer (IKA-Werke, Germany) using a 18-mm head. Finally, mixtures were poured into 3D printing syringes and stored in a fridge at 4°C. Hydrogels were designated as control, SPI2C, SPI4C, SPI6C and SPI8C, as a function of the cellulose-containing residue content. The control is the sample without residue.

2.3. Rheological assessment of hydrogels

Thermo Scientific Haake Rheostress1 Rheometer (IFI S.L., Vigo, Spain) with a serrated plate-plate geometry (35 mm in diameter) was used to measure the rheological properties of hydrogels. The space between the plates was 1 mm for all the tests. Experiments were performed at a constant temperature of 30°C.

In order to identify the critical strain and the linear viscoelastic range (LVR), strain sweeps between 0.01% and 100% strain at 1 Hz were performed. Then, frequency sweeps were carried out within the LVR between 0.01 and 50 Hz to determine the elastic and viscous moduli, G′ and G″, respectively. Furthermore, the shear flow test was

carried out from 0.1 to 50 s^{-1}. This shear sweep data were fitted to Cross model, which describes pseudoplastic flow with asymptotic viscosities at zero and infinite shear rates. Cross model[15] is represented by Equation I:

$$\eta(\dot{\gamma}) = \eta_{\infty} + \frac{\eta_0 - \eta_{\infty}}{1 + (\lambda\dot{\gamma})^m} \quad \text{(I)}$$

where η is apparent viscosity, η_{∞} is the infinite shear viscosity, η_0 is the zero shear viscosity, λ is characteristic time, $\dot{\gamma}$ is shear rate, and m is dimensionless cross rate constant, which is related to the slope.

Finally, three-interval thixotropy test was employed to determine the hydrogel recovery. In this sense, it was considered the shear rate at the syringe wall, $\dot{\gamma}_w$, which can be corrected using the Weissenberg–Rabinowitsch–Mooney equation[16]:

$$\dot{\gamma}_w = \frac{4Q}{\pi r^3} \cdot \frac{3n+1}{4n} \quad \text{(II)}$$

where Q is the volume flow rate, r is the radius of the tip, and n is the flow index calculated using the Cross model fitting, with $-m = n - 1$[17].

2.4. 3D printing

First, a cylinder with dimensions of 20 mm in diameter and 20 mm in height was designed employing a computer-aided design (CAD) software (Solid Edge, Siemens, Germany) and Ultimaker Cura 4.13.1 (Ultimaker BV, the Netherlands) as slicer. Then, hydrogels were 3D-printed by a domoBIO 2A bioprinter (Domotek, Gipuzkoa, Spain), employing a syringe extruder, a refrigerated platform and a Teflon sheet substrate. The following processing parameters were employed: nozzle size, 14 G; printing temperature, 30°C; build plate temperature, 25°C; print speed, 10 mm/s; infill density, 50%; flow, 160%; initial layer flow, 190%; and layer height, 0.5 mm.

2.5. Printability test

The shape fidelity assessment was carried out by analyzing the images of the 3D-printed products. ImageJ software was used to determine the perimeter and area of pores. The quality of the 3D-printed product was determined using shape descriptor parameters: circularity (Cr) and printability (Pr)[18]. Circularity and printability are defined according to Equations III and IV:

$$Cr = \frac{4\pi A}{P^2} \quad \text{(III)}$$

$$Pr = \frac{\pi}{4Cr} \quad \text{(IV)}$$

where A is the pore area and P is the pore perimeter.

The pores are considered perfect circles when Cr value is 1; meanwhile, perfect square pores present π/4Cr values. Moreover, a perfect lattice has a Pr value of 1.

2.6. Fourier transform infrared spectroscopy

Fourier transform infrared (FTIR) spectra of agar production residue and SPI-based 3D-printed products were performed by a Platinum-ATR Alpha II FTIR spectrometer (Bruker). A total of 32 scans were performed at a resolution of 4 cm^{-1} in the wavenumber range from 800 to 4000 cm^{-1}.

2.7. Swelling and degradation measurements

In order to calculate the swelling capacity of the 3D-printed products, different preweighed (w_p) samples were immersed into 40 mL of PBS at 37°C and then weighed again at various time points (w_t) until constant values were obtained. The swelling (S) was calculated by Equation V:

$$S = \frac{w_t - w_p}{w_p} \cdot 100 \quad \text{(V)}$$

Additionally, samples were removed after 24 h, dried in the oven at 105°C for 24 h, and weighed (w_{1d}). In order to determine the 3D-printed product degradation, Equation VI was used:

$$D = \frac{w_p - w_{1d}}{w_p} \cdot 100 \quad \text{(VI)}$$

2.8. Thermo-gravimetric analysis

Thermo-gravimetric analysis (TGA) was performed in a Mettler Toledo TGA SDTA 851 equipment (Mettler Toledo S.A.E.) under inert atmosphere conditions (10 mL N_2/min) to avoid thermo-oxidative reactions. The samples were heated from 25°C to 800°C at a heating rate of 10°C/min.

2.9. Scanning electron microscopy

The morphology of the 3D-printed products was visualized using an S-4800 field emission scanning electron microscope (SEM; Hitachi High-Technologies Corporation). Prior to observation, samples were mounted on a metal stub with double-sided adhesive tape and coated under vacuum with gold (JFC-1100) in an argon atmosphere. The 3D-printed products were analyzed employing an accelerating voltage of 5 kV.

2.10. X-ray diffraction

X-ray diffraction (XRD) study was carried out using a diffraction unit (PANalyticXpert PRO). The radiation was generated from a CuK_{α} (λ = 1.5418 Å) source (40 mA, 40 kV). Data were collected from 2θ values from 2° to 50°, where θ is the incidence angle of the X-ray beam on the 3D-printed products.

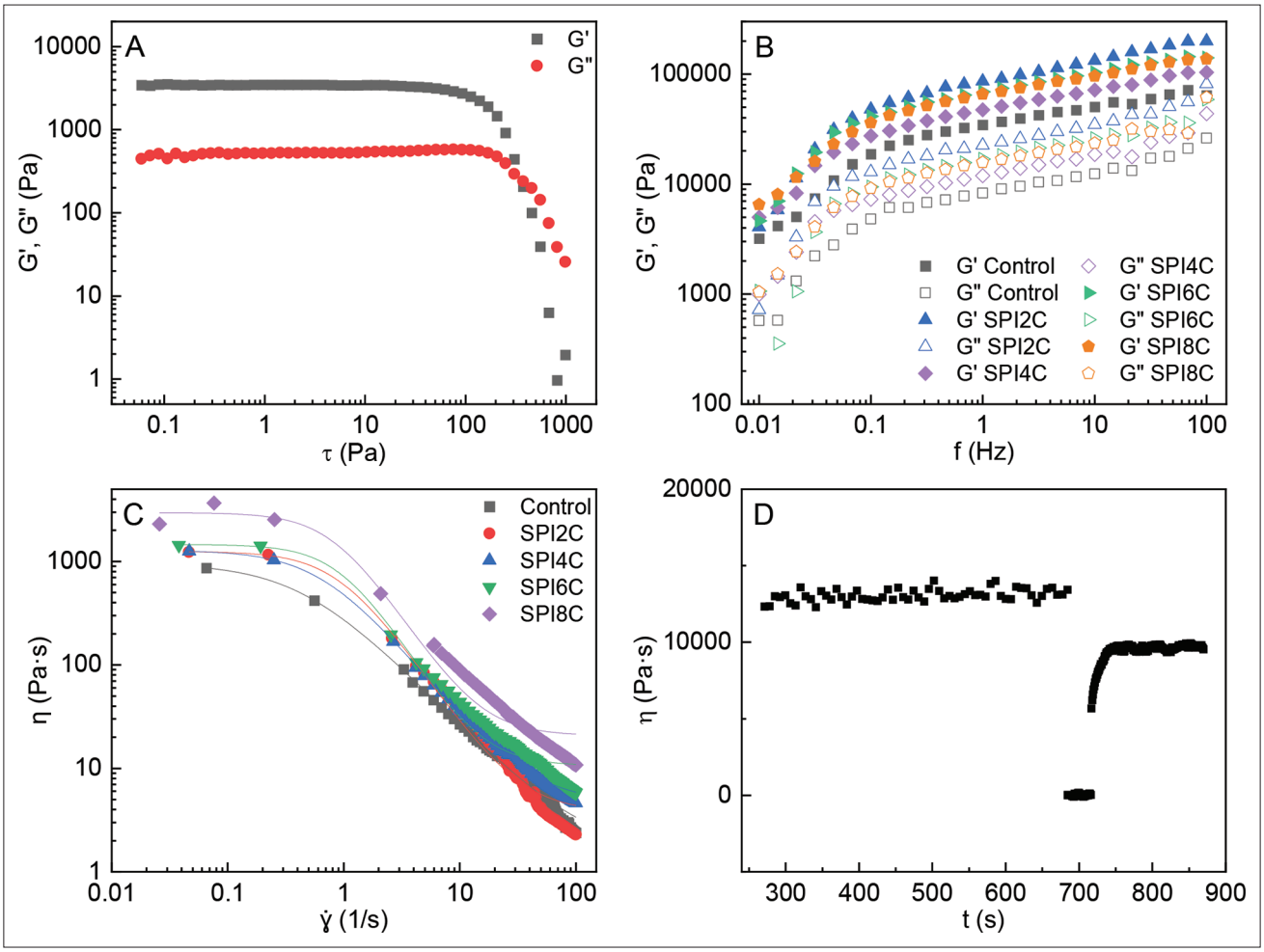

Figure 1. Rheological assessment of hydrogels. (A) Amplitude sweep for the control hydrogel. (B) Frequency sweep for the hydrogels with different cellulose contents. (C) Flow test and Cross model fitting for the hydrogels with different cellulose contents. (D) Three-interval thixotropy test for SPI8C hydrogel.

2.11. Compression tests

TA.XT.Plus C Texture Analyzer (Aname Instrumentación Científica, Madrid, Spain) was used to carry out compression tests. A 50-kg load cell was used for compression tests at 5, 10, 20, and 50% strain, while a 5-kg load cell was employed for a two-cycle compression-decompression tests at 20% strain. Data were collected at 1 mm/s and 1 g trigger force. In order to analyze the mechanical behavior of 3D-printed product, samples were conditioned in a controlled chamber at 23°C and 100% relative humidity before testing.

2.12. Statistical analysis

One-way analysis of variance (ANOVA) was used to determine the significance of differences among samples. The analysis was performed with a SPSS computer program (SPSS Statistic 28.0) and Tukey's test was used for post hoc multiple comparisons. All the assays were done, at least, in triplicate. Differences were statistically significant at $p < 0.05$.

3. Results and discussion

3.1. Rheological and printability assessments

Rheological properties of hydrogels substantially influence the 3D printing process. Therefore, amplitude sweep, frequency sweep, flow, and three-interval thixotropy test were performed. First, the linear viscoelastic region (LVR) was identified by performing an amplitude sweep and analyzing the trend of storage (G′) and loss (G″) moduli. All samples showed the same trend, and the control sample is shown in Figure 1A. Within LVR region, G′ and G″ values are independent of the strain, microstructure is maintained intact, and any disruption is instantaneously recovered[19]. Hydrogels showed solid-like behavior with values of G′ higher than those of G″. LVR finished when the moduli crossover (G′ = G″) occurred, and thus, any microstructure disturbance produces irreversible deformations in the gel network structure[20]. G′ and G″ joined at high oscillation stress values, around 300 Pa;

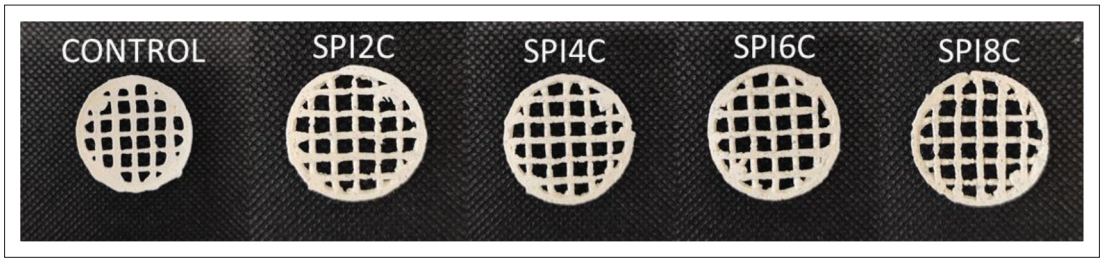

Figure 2. Photographs of 3D-printed products with different cellulose contents.

therefore, this large LVR favors the shape fidelity of 3D printing samples[21].

After LVR determination, a frequency sweep analysis was conducted within the LVR (Figure 1B). G′ and G″ moduli change slightly at different frequencies and in the entire range of frequency sweep inks showed higher G′ than G″, and thus, tan $\delta < 1$, indicating solid-like behavior or elastic behavior. These slight differences as well as moderate low loss tangent values denoted the character of weak gels. Additionally, the incorporation of cellulose slightly increased G′ and G″ values, suggesting a more robust and tighter intermolecular network formed by protein-polysaccharide interactions[22]; however, no clear trend was found with increasing cellulose content, in accordance with the similar microstructure observed for all the cellulose-containing samples by SEM analysis.

Regarding flow test (Figure 1C), results showed that viscosity values decreased when shear rate increased, indicating that inks showed shear-thinning or pseudo-plastic behavior, an ideal property for 3D printing technique[23]. Increasing cellulose content led to higher viscosity values. Specifically, the viscosity values were around 3, 5, 6, and 12 Pa·s for SPI2C, SPI4C, SPI6C, and SPI8C, respectively, at the syringe wall shear rate (90 s^{-1}). Therefore, 8 wt % was the maximum content to ensure printability, since hydrogels with a higher cellulose content offer more resistance to the printing process and make the material extrusion via the nozzle difficult.

Finally, the three-interval thixotropy test, which mimics extrusion-based printing, was carried out for all the samples and since the hydrogel recovery measured was higher for SPI8C sample, the performance of this sample is shown in Figure 1D. The hydrogel was found to recover viscosity and rebuild the broken crosslinks after rest, retaining their shape after printing. The recovery values after 60 s were around 70%, with SPI8C showing the highest recovery result of 78%. In order to achieve a good shape fidelity during printing, the deposited hydrogel should exhibit a fast recovery rate, with an immediate restoration of the elastic behavior of the material and the exclusion of continuous flow (spreading)[20]. Therefore, the hydrogels developed should have the capacity to flow and recover their structure, which is a property required for 3D printing.

Table 1. Circularity (Cr) and printability (Pr) values for 3D-printed products

	Cr	Pr
Control	0.76 ± 0.01^{a}	1.04 ± 0.02^{a}
SPI2C	0.74 ± 0.02^{b}	1.06 ± 0.03^{b}
SPI4C	0.72 ± 0.02^{c}	1.09 ± 0.03^{c}
SPI6C	$0.73 \pm 0.01^{b,c}$	$1.07 \pm 0.02^{b,c}$
SPI8C	0.72 ± 0.02^{c}	1.09 ± 0.03^{c}

[a-c] Two means followed by the same letter in the same column are not significantly different ($p > 0.05$).

Although there is no consensus on how to grade printability and objectively/quantitatively describe shape fidelity[24], based on the rheological results obtained, it could be concluded that the 3D-printed products prepared in this work present good shape fidelity (Figure 2). In this sense, geometrical descriptors (Cr and Pr) were used to analyze pores and to relate their dimensions to the intended CAD designs, since it is of crucial importance that the printed objects closely match the original computer-designed object. With this purpose, different images of 3D-printed products were analyzed by ImageJ software. As can be seen in Table 1, Cr and Pr values changed ($p < 0.05$) with different contents of cellulose, with the control being the only sample that exhibited the nearest results to perfect square pores, which are Cr = π/4 and Pr = 1. It is worth noting that all samples showed suitable printability values in the range of 0.9–1.1[25].

3.2. Physicochemical and thermal properties

First, the agar production residue was analyzed by FTIR (Figure 3A). This residue showed an intense peak at 1030 cm^{-1}, attributed to C–O and C–O–C vibrations of the 3,6-anhydrogalactose bridge, as well as to the glycosidic linkage[26]. Agarose characteristic bands were also observed at 933 and 876 cm^{-1}, attributed to the 3,6-anhydro-β-galactose skeletal bending modes. The absorption band located at 1634 cm^{-1} was related to the protein[27] and

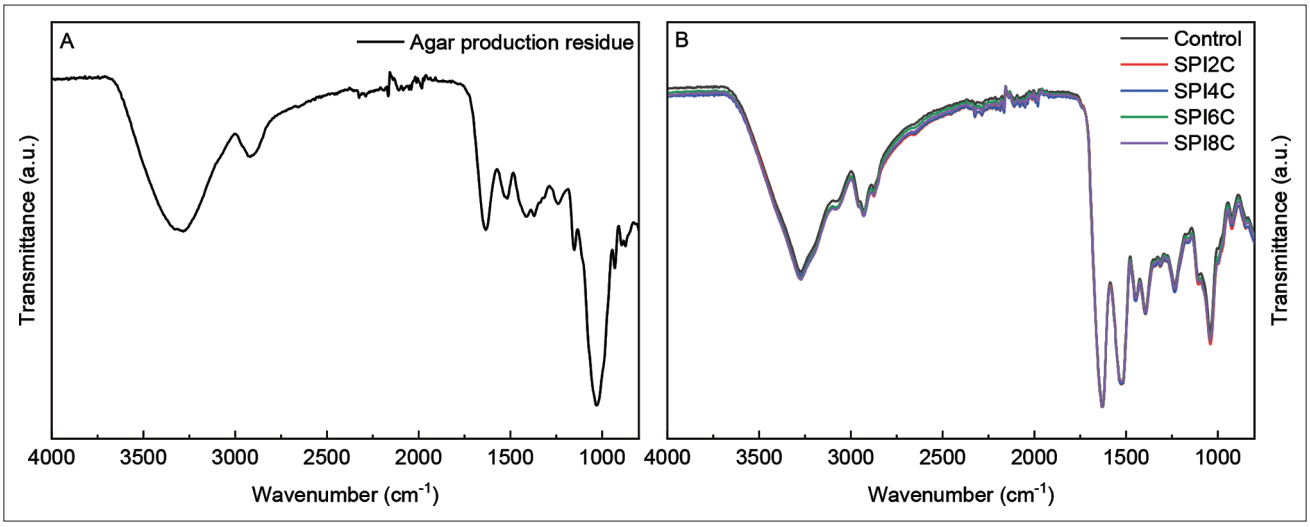

Figure 3. FTIR spectra for (A) agar production residue and (B) for 3D-printed products.

Table 2. Swelling capacity at 5 h and 24 h and degradation at 24 h for 3D-printed products

	Swelling capacity at 5 h (%)	Swelling capacity at 24 h (%)	Degradation at 24 h (%)
Control	454 ± 37[a]	484 ± 42[a]	35 ± 8[a]
SPI2C	396 ± 12[ab]	417 ± 32[ab]	37 ± 5[a]
SPI4C	406 ± 8[ab]	425 ± 10[ab]	38 ± 2[a]
SPI6C	408 ± 28[ab]	429 ± 33[ab]	32 ± 2[a]
SPI8C	385 ± 20[b]	398 ± 17[b]	37 ± 5[a]

[a-b] Two means followed by the same letter in the same column are not significantly different ($p > 0.05$).

the weak band observed at 1241 cm^{-1} could be assigned to the pyranose ring bending vibrations in agarose. The broad band between 3000 and 3500 cm^{-1} was associated to the OH groups responsible for hydrogen bonding in the cellulose molecule[28]. It is worth noting the absence of the bands around 1726 cm^{-1} due to the lack of lignin in this type of algae waste.

FTIR spectra of 3D-printed products are presented in Figure 3B, where the characteristic bands of proteins (SPI and gelatin), related to amide I (1630 cm^{-1}), amide II (1527 cm^{-1}), and amide III (1236 cm^{-1}), were observed[29,30]. The main absorption bands of glycerol appeared at 800–1150 cm^{-1} and are related to the vibrations of C–C and C–O bonds[31]. The addition of cellulose did not lead to formation of new bands; therefore, no chemical reaction between proteins and cellulose occurred, although the slight increase of the broad band at 3500–3000 cm^{-1} suggested H-bonding among polar groups of proteins and hydroxyl groups of cellulose. This was confirmed by the swelling test results (Table 2), since control samples

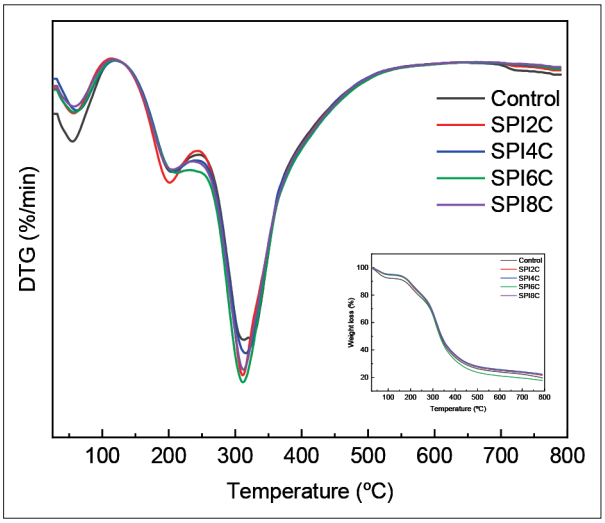

Figure 4. DTG curves (weight loss in the inlet) for 3D-printed products with different cellulose content.

had the highest swelling values, while SPI8C showed the lowest values ($p < 0.05$) at around 400%. These values are of great importance since high swelling capacity is needed for some applications, such as wound healing, in order to absorb wound exudates[32]. All samples showed a fast PBS uptake and swelling was slower after 5 h of immersion, until a plateau was reached at 24 h. Furthermore, in contrast to the results reported in the literature for SPI 3D-printed products[33], samples in this work preserved their integrity during immersion in PBS at 37°C and the weight loss was in the 30%–40% range for all samples ($p > 0.05$).

Regarding thermal stability, derivative thermogravimetric (DTG) curves are shown in Figure 4. There

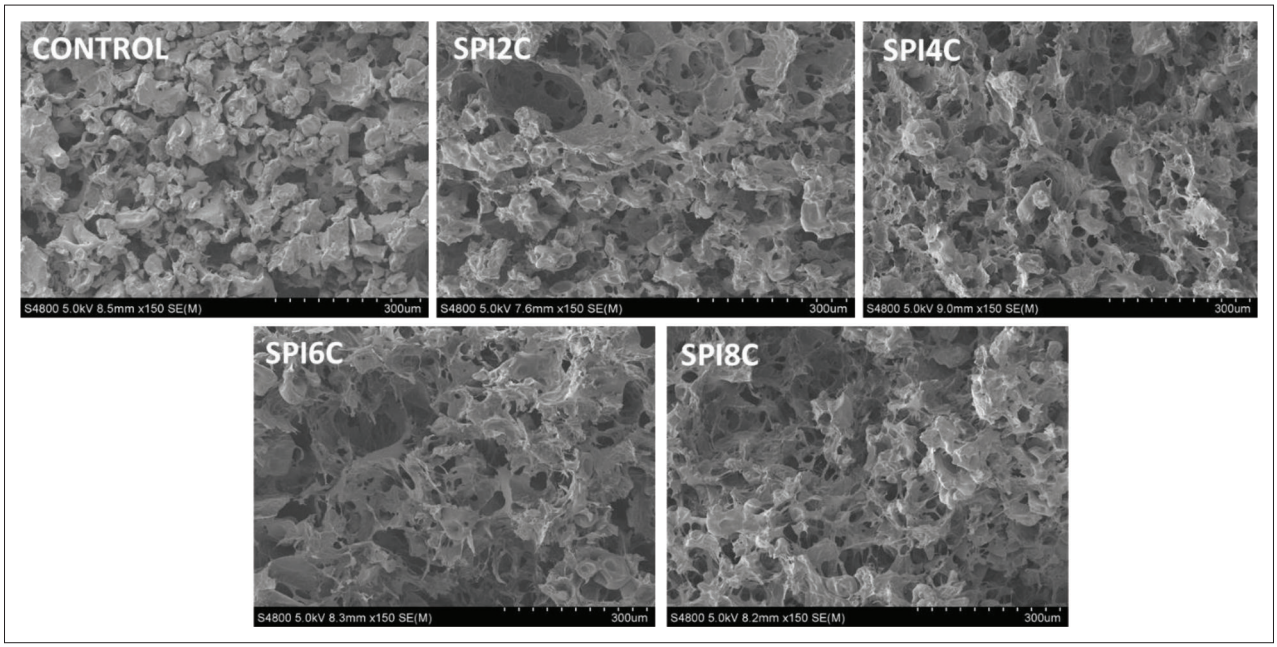

Figure 5. SEM images of 3D-printed products with different residue contents.

are three main weight loss steps for all the samples, regardless of the cellulose content. The first one, which occurs at temperatures lower than 100°C, is associated to water evaporation[34] and its value was lower than 10%. The second weight loss step appeared around 200°C and it is mainly related to the evaporation of glycerol[35], but also to the initial cellulose depolymerization[36] and to the unstable chemical bond breaks in soy protein[37]. The last step appeared around 310°C and corresponds to cellulose[36], SPI[37], and gelatin[38] decomposition. As expected, there was no peak around 400°C corresponding to the degradation of lignin. Considering thermal analysis, it can be said that 3D-printed products were endowed with thermal stability, which broadens their applicability.

3.3. Morphology and mechanical properties

In order to study the morphology of 3D-printed products, SEM images were analyzed (Figure 5). All samples featured a porous structure with randomly distributed pores of varying sizes and shapes. The microstructure was more loosened when cellulose was incorporated, but no specific trend was found with increasing cellulose content. It is worth noting that cellulose-containing 3D-printed products did not show aggregates, indicating that cellulose was well-distributed. This was corroborated by XRD patterns (Figure 6), which exhibited two broad peaks at 9° and 20°. The first peak was associated to the α-helix of soy protein as well as to the triple-helix of gelatin. The second peak was attributed to the β-sheet structure of the soy protein, the single left-handed helix chain of gelatin,

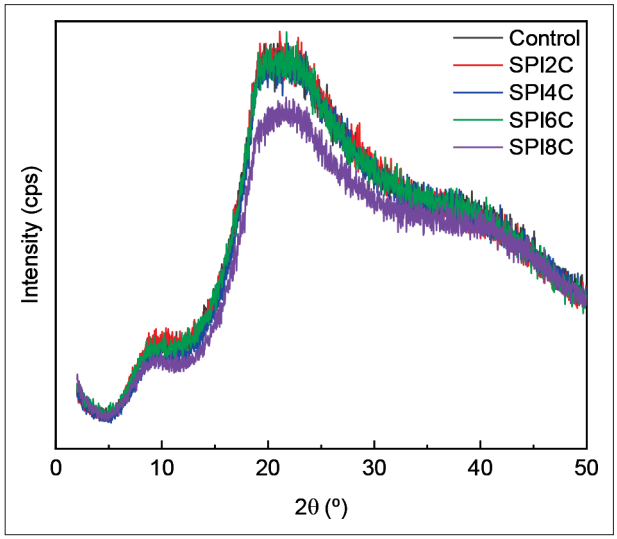

Figure 6. XRD patterns of 3D-printed products with different residue contents.

and the cellulose structure[39-41]. Interactions between biopolymers decreased protein–protein intramolecular interactions, leading to more amorphous structures, as evidenced in SPI8C, which have the highest cellulose content employed in this work.

Regarding mechanical properties, it is worth noting that 3D-printed products did not display ruptures, even at a compression strain of 50%. Both elastic modulus (Figure 7A) and force (Figure 7B) increased with the increase of cellulose content ($p > 0.05$), showing suitable values for applications such as wound healing[42].

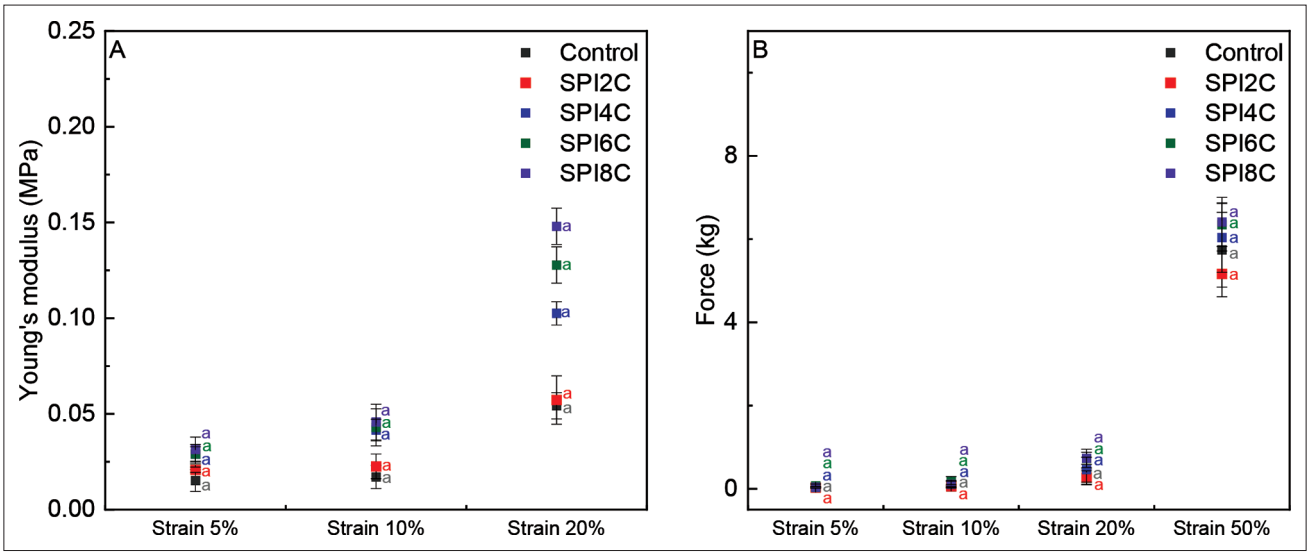

Figure 7. Elastic modulus and force values at different strains for 3D-printed products.
[a]Two means followed by the same letter at the same strain are not significantly different ($p > 0.05$).

Furthermore, texture profile analysis provides information on the hardness and cohesiveness of the hydrogels, which are highly relevant for analyzing their workability for 3D printing. In this sense, hardness, which is the maximum force required to produce the first deformation, showed a value of 1004 ± 43 g for the control hydrogel. The hardness increased with the addition of agar residue up to 1389 ± 52 g for the SPI8C hydrogel. Regarding cohesiveness, which is related to the ability of a gel to maintain its own structure under compressive stress, the control hydrogel showed a high cohesive value of 0.858 ± 0.014, which remained nearly constant with residue addition (0.843 ± 0.021 for SPI8C), indicating a high ability to maintain 3D structural integrity and thus structure after printing, as demonstrated by rheological analysis. This mechanical behavior revealed that 3D-printed products do not break under compression and maintain mechanical integrity; therefore, they are strong enough not to be damaged by handling or replacement.

4. Conclusion

Agar production residue was used without further purification in order to reduce the carbon footprint associated to the manufacture of products based on valorized polymers. This residue is mainly constituted by cellulose and was used as a filler in soy protein-based inks. The rheological assessment revealed that the hydrogels have shear-thinning behavior, which is favorable for 3D printing, as well as suitable printability values. The use of cellulose as a filler in soy protein hydrogels led to hydrogen bonding between the polar groups of protein and the hydroxyl groups of cellulose, resulting in 3D-printed products with high swelling capacity with their integrity preserved under physiological conditions. Additionally, 3D-printed products showed thermal stability up to 200°C. Furthermore, morphological evaluation showed that cellulose was well distributed in the protein matrix, since no aggregate was observed by SEM, resulting in 3D-printed products that maintain their integrity even at a compression strain of 50% and display a shape recovery behavior in compression-decompression cycles. Considering the swelling capacity of the 3D-printed products at physiological conditions and the mechanical performance of the hydrated 3D-printed products, the suitability of these products for biomedical applications could be assessed.

Acknowledgments

None.

Funding

This work was supported by a grant PID2021-124294OB-C22 funded by MCI/AEI10.13039/501100011033 and by "ERDF A way of making Europe." This work was also supported by the Basque Government (IT1658-22). J.U. thanks the University of the Basque Country (ESPDOC21/74) and T.C. thanks the Basque Government (PRE_2022_2_0005) for their fellowships.

Conflict of interest

The authors declare they have no competing interests.

Author contributions

Conceptualization: Pedro Guerrero, Koro de la Caba
Formal analysis: Jone Uranga
Funding: Koro de la Caba
Investigation: Jone Uranga, Teresa Carranza, Miriam Peñalba
Methodology: Teresa Carranza, Miriam Peñalba, Pedro Guerrero
Project administration: Pedro Guerrero, Koro de la Caba
Resources: Koro de la Caba
Supervision: Pedro Guerrero, Koro de la Caba
Writing – original draft: Jone Uranga
Writing – review & editing: Teresa Carranza, Miriam Peñalba, Pedro Guerrero, Koro de la Caba

Ethics approval and consent to participate

Not applicable.

Consent for publication

Not applicable.

Availability of data

Data will be made available on reasonable request.

References

1. Jayanthi Antonisamy A, Marimuthu M, Malayandi S *et al.*, 2023, Sustainable approaches on industrial food wastes to value-added products—A review on extraction methods, characterizations, and its biomedical applications. *Environ Res,* 217:114758.
2. Oliver-Simancas R, Labrador-Fernández L, Díaz-Maroto MC, *et al.*, 2021, Comprehensive research on mango by-products applications in food industry. *Trends Food Sci Technol,* 118:179–188.
3. Ren C, Wu S, Wang W, *et al.*, 2023, Recycling of hazardous and industrial solid waste as raw materials for preparing novel high-temperature-resistant sulfoaluminate-magnesia aluminum spinel cement. *J Build Eng,* 64:105550.
4. Bertasa M, Dodero A, Alloisio M, *et al.*, 2020, Agar gel strength: A correlation study between chemical composition and rheological properties. *Eur Polym J,* 123:109442.
5. Trigueros E, Sanz MT, Filipigh A, *et al.*, 2021, Enzymatic hydrolysis of the industrial solid residue of red seaweed after agar extraction: Extracts characterization and modelling. *Food Bioprod Process,* 126:356–366.
6. Li Z, Hu Q, Chen J, *et al.*, 2022, Optimized strategy for simultaneous recovering bioactive oligosaccharides and reusable perlite from agar industrial waste residues. *J Clean Prod,* 378:134631.
7. Martínez-Sanz M, Cebrián-Lloret V, Mazarro-Ruiz J, *et al.*, 2020, Improved performance of less purified cellulosic films obtained from agar waste biomass. *Carbohydr Polym,* 233:115887.
8. Haldar D, Purkait MK, 2020, Micro and nanocrystalline cellulose derivatives of lignocellulosic biomass: A review on synthesis, applications and advancements. *Carbohydr Polym,* 250:116937.
9. Jiang S, Zhang T, Song Y, *et al.*, 2019, Mechanical properties of whey protein concentrate based film improved by the coexistence of nanocrystalline cellulose and transglutaminase. *Int J Biol Macromol,* 126:1266–1272.
10. Barty-King CH, Chan CLC, Parker RM, *et al.*, 2021, Mechanochromic, structurally colored, and edible hydrogels prepared from hydroxypropyl cellulose and gelatin. *Adv Mater,* 33:2102112.
11. Wu M, Wu P, Xiao L, *et al.*, 2020, Biomimetic mineralization of novel hydroxyethyl cellulose/soy protein isolate scaffolds promote bone regeneration in vitro and in vivo. *Int J Biol Macromol,* 162:1627–1641.
12. Quan H, Zhang T, Xu H, *et al.*, 2020, Photo-curing 3D printing technique and its challenges. *Bioact Mater,* 5:110–115.
13. Jing L, Sun J, Liu H, *et al.,* 2021, Using plant proteins to develop composite scaffolds for cell culture applications. *Int J Bioprint,* 7:66–77.
14. Chen J, Mu T, Goffin D, *et al.*, 2019, Application of soy protein isolate and hydrocolloids based mixtures as promising food material in 3D food printing. *J Food Eng,* 261:76–86.
15. Cheng Y, Fu Y, Ma L, *et al.*, 2022, Rheology of edible food inks from 2D/3D/4D printing, and its role in future 5D/6D printing. *Food Hydrocoll,* 132:107855.
16. Calafel I, Aguirresarobe RH, Peñas MI, *et al.*, 2020, Searching for rheological conditions for FFF 3D printing with PVC based flexible compounds. *Materials,* 13:178.
17. Carranza T, Zalba-Balda M, Baraibar MJB, *et al.*, 2022, Effect of sterilization processes on alginate/gelatin inks for three-dimensional printing. *Int J Bioprint,* 9:309–319.
18. Liu Q, Jain T, Peng C, *et al.,* 2020, Introduction of hydrogen bonds improves the shape fidelity of viscoelastic 3D printed scaffolds while maintaining their low-temperature printability. *Macromolecules,* 53:3690–3699.
19. Simões A, Miranda M, Cardoso C, *et al.*, 2020, Rheology by design: A regulatory tutorial for analytical method validation. *Pharmaceutics*, 12:820.
20. Parimita S, Kumar A, Krishnaswamy H, *et al.*, 2023, Solvent triggered shape morphism of 4D printed hydrogels. *J Manuf Process,* 85:875–884.
21. Chen M, Yang L, Zheng Y, *et al.*, 2021, Rheological behaviors and structure build-up of 3D printed polypropylene and

polyvinyl alcohol fiber-reinforced calcium sulphoaluminate cement composites. *J Mater Res Technol,* 10:1402–1414.

22. Yu J, Wang X, Li D, *et al.*, 2022, Development of soy protein isolate emulsion gels as extrusion-based 3D food printing inks: Effect of polysaccharides incorporation. *Food Hydrocoll,* 131:107824.

23. Liu Z, Zhang M, Bhandari B, *et al.*, 2018, Impact of rheological properties of mashed potatoes on 3D printing. *J Food Eng,* 220:76–82.

24. Schwab A, Levato R, D'Este M, *et al., 2020,* Printability and shape fidelity of bioinks in 3D bioprinting. *Chem Rev,* 120:11028–11055.

25. Ouyang L, Yao R, Zhao Y, *et al.*, 2016, Effect of bioink properties on printability and cell viability for 3D bioplotting of embryonic stem cells. *Biofabrication,* 8:035020.

26. Liu X, Renard CMGC, Bureau S, *et al.*, 2021, Revisiting the contribution of ATR-FTIR spectroscopy to characterize plant cell wall polysaccharides. *Carbohydr Polym,* 262:117935.

27. Paniz OG, Pereira CMP, Pacheco BS, *et al.,* 2020, Cellulosic material obtained from Antarctic algae biomass. *Cellulose*, 27:113–126.

28. Jmel MA, Anders M, Messaoud GB, *et al.,* 2019, The stranded macroalga Ulva lactuca as a new alternative source of cellulose: Extraction, physicochemical and rheological characterization. *J Clean Prod,* 234:1421–1427.

29. Mansour M, Salah M, Xu X, 2020, Effect of microencapsulation using soy protein isolate and gum arabic as wall material on red raspberry anthocyanin stability, characterization, and simulated gastrointestinal conditions. *Ultrason Sonochem,* 63:104927.

30. Casanova F, Mohammadifar MA, Jahromi M, *et al.,* 2020, Physico-chemical, structural and techno-functional properties of gelatin from saithe (*Pollachius virens*) skin. *Int J Biol Macromol,* 156:918–927.

31. Basiak E, Lenart A, Debeaufort F, 2018, How glycerol and water contents affect the structural and functional properties of starch-based edible films. *Polymers,* 10:412.

32. Heras KL, Santos-Vizcaino E, Garrido T, *et al.,* 2020, Soy protein and chitin sponge-like scaffolds: from natural by-products to cell delivery systems for biomedical applications. *Green Chem,* 22:3445–3460.

33. Varshney N, Saji AK, Poddar S, *et al.,* 2022, Freeze–thaw-induced physically cross-linked superabsorbent polyvinyl alcohol/soy protein isolate hydrogels for skin wound dressing: In vitro and in vivo characterization. *ACS Appl Mater Interfaces,* 14:14033–14048.

34. Zhang H, Wang L, Li H, *et al.,* 2021, Changes in properties of soy protein isolate edible films stored at different temperatures: Studies on water and glycerol migration. *Foods,* 10:1797.

35. Mazurek P, Ekbrant BEF, Madsen FB, *et al.*, 2019, Glycerol-silicone foams—Tunable 3-phase elastomeric porous materials. *Eur Polym J,* 113:107–114.

36. Nurazzi NM, Asyraf MRM, Rayung M, *et al.,* 2021, Thermogravimetric analysis properties of cellulosic natural fiber polymer composites: A review on influence of chemical treatments. *Polymers,* 13:2710.

37. Xu Y, Han Y, Chen M, *et al.,* A soy protein-based film by mixed covalent cross-linking and flexibilizing networks. *Ind Crops Prod,* 183:114952.

38. Yavari Maroufi L, Ghorbani M, Tabibiazar M, 2020, A gelatin-based film reinforced by covalent interaction with oxidized guar gum containing green tea extract as an active food packaging system. *Food Bioprocess Technol,* 13:1633–1644.

39. Lethesh KC, Evjen S, Venkatraman V, *et al,*, 2020, Highly efficient cellulose dissolution by alkaline ionic liquids. *Carbohydr Polym,* 229:115594.

40. Dai H, Li X, Du J, *et al.,* 2020, Effect of interaction between sorbitol and gelatin on gelatin properties and its mechanism under different citric acid concentrations. *Food Hydrocoll,* 101:105557.

41. Dorishetty P, Balu R, Sreekumar A, *et al.,* 2019, Robust and tunable hybrid hydrogels from photo-cross-linked soy protein isolate and regenerated silk fibroin. *ACS Sustain Chem Eng,* 7:9257–9271.

42. Norahan MH, Pedroza-González SC, Sánchez-Salazar MG, *et al.*, 2023, Structural and biological engineering of 3D hydrogels for wound healing. *Bioact Mater,* 24:197–235.